01 Jan 1973

Use of the Split-Film Sensor to Measure Turbulence in Water near a Wall

Paul H. Blinco

V. A. Sandborn

USE OF THE SPLIT-FILM SENSOR TO MEASURE TURBULENCE IN WATER NEAR A WALL

P. H. Blinco
Stone and Webster Engineering Corporation
Greenwood Plaza
Denver, Colorado 80217

V. A. Sandborn
Department of Civil Engineering
Colorado State University
Fort Collins, Colorado 80521

ABSTRACT

Because of its small size and unique design, the 0.15-mm diameter split-film sensor has many significant advantages over the conventional X-configuration hot-film sensor and the yaw-wire technique for measuring turbulence near a wall. Calibration of the split-film sensor indicates that the magnitude and yaw angle of the instantaneous velocity vector is dependent only on the sum and ratio of the sensor outputs, respectively. Results of limited measurements of the longitudinal and vertical turbulence intensities and Reynolds stress for hydraulically smooth, free surface flows are presented. Digital time series of the split-film outputs revealed the following information: (1) the split-film sensor longitudinal and vertical turbulence intensities and Reynolds stress compares favorably with previous studies; (2) the split-film sensor can be used as an instantaneous velocity vector transducer; (3) the split-film sensor is capable of making two-dimensional turbulence measurements in water to within five probe diameters of the wall. Calibration and experimental results indicate that the split-film sensor may be useful in improved spatial definition of the turbulent structure in wall shear flows.

INTRODUCTION

In previous studies of water turbulence near walls, relatively large hot-film sensors were used. Data obtained by using large hot-film sensors such as the X-array and yaw technique are difficult to interpret because of direct heat transfer from the sensor to the wall and the non-linear heat transfer across the sensor's length in shear flows. To obtain better spatial definition of the turbulent velocity statistics in the wall region, researchers have either altered the fluid properties or resorted to using highly viscous fluids, such as Bakewell and Lumley(1) and Eckelmann and Reichardt (4). The approach involving reduction of the size of the sensor is restricted by the structural strength of the sensor and dynamic loading of fluid flow.

With the recent development of the split-film hot-film (SFHF) sensor, it is now possible to obtain measurements closer to the wall than was previously possible with the X-array sensor. Because of its small size and unique design, the SFHF sensor has many advantages over the conventional two-dimensional velocity sensors. Aside from improved spatial definition, the SFHF sensor is very versatile and may also be used as an instantaneous velocity vector probe or as an X-array sensor. The SFHF sensor in the instantaneous vector mode is very useful for making a digital time series analysis of the longitudinal and vertical velocity fluctuations.

Two recent studies have reported some operational details on the SFHF sensor, as well as some limited turbulence measurements in air. Olin and Kiland (9) were the first to study the heat transfer relations of the SFHF sensor under dynamic calibration conditions. Their study was concerned primarily with the calibration and the functional form of the heat transfer relations of the SFHF sensor. Olin and Kiland concluded that the magnitude of the two-dimensional instantaneous velocity vector and yaw angle are functions of the sum and ratio of the

heat transfer from the two isolated sensors, respectively. Spencer and Jones (11) have studied extensively the heat transfer relations around a heated split-film cylinder in a cross flow. From theoretical considerations they were able to develop an operational response function for the SFHF sensor when it is used in X-array mode. The purpose of their study was to determine and compare the results obtained with different sized SFHF sensors (0.051 mm, 0.153 mm) and results obtained by conventional boundary layer sensors. They found that the longitudinal and vertical turbulence intensities and Reynolds stress obtained with the SFHF sensor were in general agreement with the intensities and shear stress obtained in previous studies in air. Spencer and Jones noted that as the wall was approached, the SFHF sensor data began to deviate from Klebanoff's (6) results at about $y^+ = 150$. This discrepancy appears to be the result of probe interference or heat transfer to the wall from the adjacent split film sensor or both. Spencer and Jones concluded that the SFHF sensor is capable of measuring the two-dimensional velocity field within 10 probe diameters from the wall.

Some recent experimental results obtained in a 10-meter long by 20.4 cm wide open channel flume are summarized in this paper. The operation theory, calibration, and statistical results obtained by using a 0.153 mm SFHF sensor in instantaneous velocity vector mode near a smooth wall are discussed.

THEORY OF OPERATION

The principle of operation of the SFHF sensor is based on the non-uniform heat transfer distribution around a constant temperature cylinder in a cross flow as shown in Figure 1. A typical SFHF sensor consists of a 0.153 mm diameter, 1.01 mm-long active sensor made of 1000 Å platinum film which is deposited on a 2.04 mm-long quartz rod. This film is split into independent sensors along a plane which is parallel to the mean flow and perpendicular to the wall as shown in Figure 2. The split film is coated with quartz to provide electrical isolation when in an electrically conducting fluid. The individual film segments are heated to equal constant temperature by a two-channel constant temperature anemometer.

In the development of the response equations it is assumed that the heat transfer distribution changes instantaneously with changes in the velocity field and that heat transfer along the cylinder's axis is negligible compared with the radial heat transfer. The latter assumption is valid for cylindrical hot-film sensors with modest length-to-diameter ratios. It is also further assumed that the turbulence scale has negligible effect on the heat transfer characteristics. This appears to be valid for moderate ratios of turbulent microscale to sensor diameter (10).

Considering the velocity field as shown in Figure 1, the effective instantaneous velocity vector, q is given by

$$q = \{(\overline{U} + u)^2 + v^2 + w^2\}^{1/2} \qquad (1)$$

where $\overline{U}$ = the temporal mean value of the longitudinal velocity and where u, v and w are fluctuating components in the longitudinal, vertical and transverse directions, respectively. Here it is assumed that the mean velocity is a function of the vertical coordinate, y, alone. The sum of the convective heat transfer from the axially split sensors, E_S^*, has been shown (9) to be related to the magnitude of the velocity, q, in the form

$$E_S^* = (A_S + B_S\, q^n)\, f(\theta) \qquad (2)$$

where

$$E_S^* = \frac{\alpha_1 E_1^2 R_{01}}{R_1(R_1 - R_{01})} + \frac{\alpha_2 E_2^2 R_{02}}{R_2(R_2 - R_{02})} \qquad (3)$$

E_i (i = 1, 2) is the individual split-film voltage potential, α_i is the coefficient of thermal resistance, and R_i and R_{0i} are the electrical resistances at operating and ambient temperatures, respectively, and $f(\theta)$ is an arbitrary function of the yaw angle, θ. The coefficients A_S, B_S and n are calibration constants to be determined. Using the assumption that heat transfer due to fluctuations along the sensor axis is small compared with the radial heat transfer, Equation 2 reduces to the response equation for the magnitude of the instantaneous velocity vector in the plane normal to the sensor axis, Figure 2. The form of Equation 2 is the same as proposed by Spencer and Jones (11), whereas Olin and Kiland (9) assumed that E_S^* was a function of q alone.

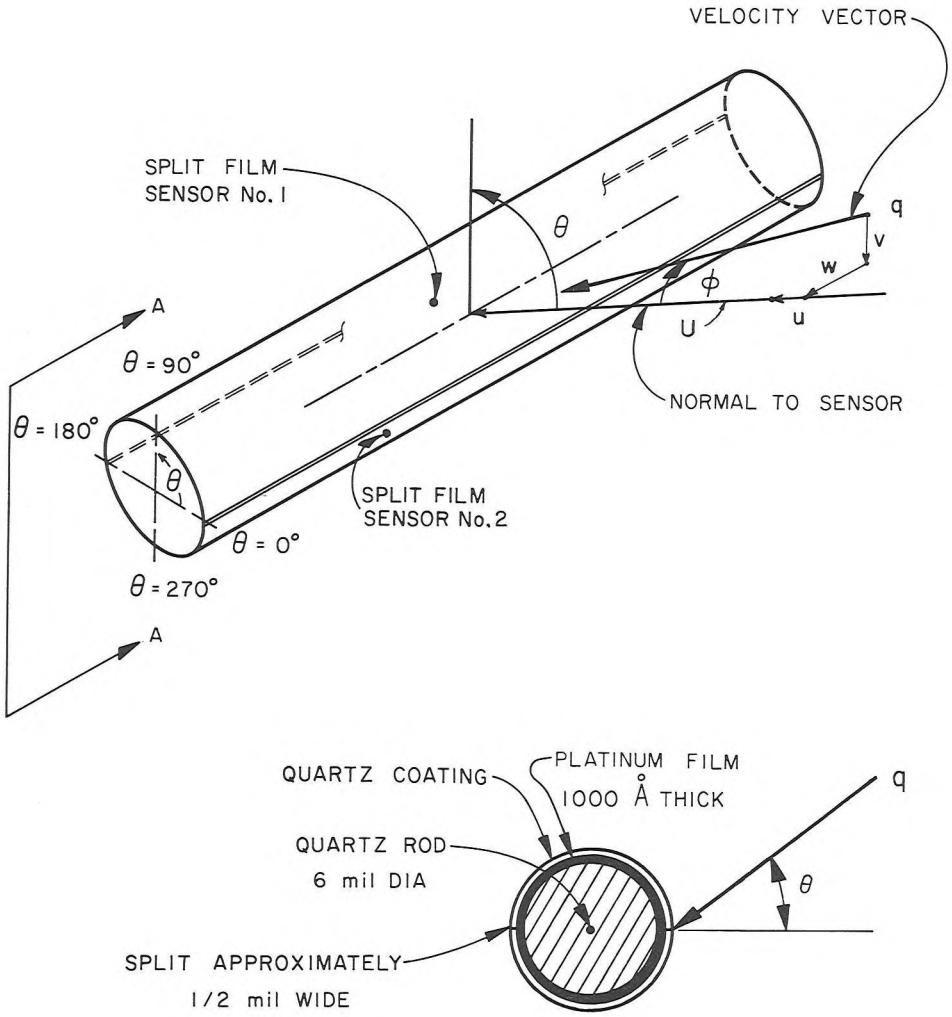

Figure 1. Definition sketch of SFHF sensor.

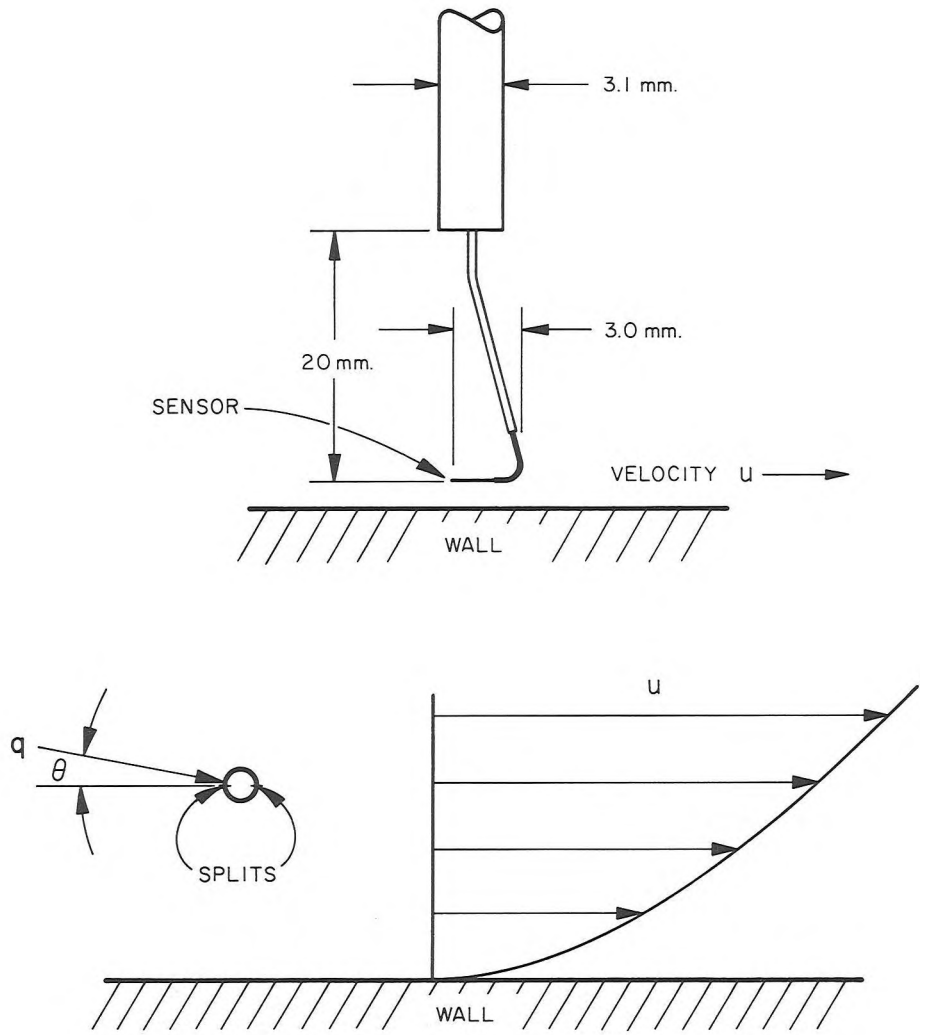

Figure 2. Schematic of the SFHF sensor orientation to wall.

It has been found that the convective heat transfer distribution around the SFHF sensor is dependent on the yaw angle, θ (9). For two perfectly matched sensors, the heat transfer for a given sensor is maximum when the stagnation point is located at $\theta = \pm \pi/2$. Likewise if the stagnation point is at $\theta = 0, \pi$, the sensor outputs would be equal. This suggests that the yaw angle, θ, would vary with respect to the ratio of sensor outputs, E_R^*, in the empirical representation

$$E_R^* = (A_R + B_R \theta^n) f(q) \tag{4}$$

where

$$E_R^* = \frac{\dfrac{\alpha_1 E_1^2 R_{01}}{R_1(R_1 - R_{01})}}{\dfrac{\alpha_2 E_2^2 R_{02}}{R_2(R_2 - R_{02})}} \tag{5}$$

where A_R, B_R are calibration constants and $f(q)$ indicates an arbitrary functional relationship. E_R^* is assumed to be a function of both θ and q.

Because it is practically impossible to manufacture two sensors perfectly matched with respect to geometry and electrical characteristics, it is equally unlikely that two sensors will be at the same temperature when operated. Under most operating conditions, sensor temperatures will be slightly different, thus causing heat transfer between the split films. For example, the coefficients of thermal resistance, α_i, for the TSI model 1280-TW, 0.153 mm-diameter SFHF sensors used in this study were found to be 2.00×10^{-3} and $1.95 \times 10^{-3}/C^{o}$. Using an over heat ratio of 1.06, this would give a temperature differential of 2°C between the sensors. During these experiments, the SFHF sensors were operated at different heat ratios. This was done to minimize the heat transfer between the two sensors. To our knowledge, no data are available showing the effects of thermal heat transfer between axially segmented sensors and the thermal feedback from the substratum to the sensors.

SPLIT-FILM CALIBRATION

A series of calibrations were performed to establish the validity and limits of Equations 2 and 4. The SFHF sensor was calibrated in a constant-head jet tank designed for this purpose. This calibration system consisted of a cylindrical chamber with a 0.95-cm diameter internally rounded orifice supplied by a constant-head tank. By a series of valves, the jet flow was regulated over a jet velocity range of 15 to 95 cm/sec. The SFHF sensor could be rotated $\pm$ 45° in 2° increments. Details of the calibration system can be found in Reference 2. Results of the SFHF sensor calibration are summarized in Figs. 3, 4, 5, and 6. The results presented in Figures 3 to 6 consist of six independent calibrations performed during a 16-day period. We wish to demonstrate here the ability of the SFHF sensor to "hold" its calibration under varying conditions. Given on each figure is the least square regression curve for the data sample size N_S, the regression coefficient, ρ_r, an the standard error of the sample, ε. For the sake of clarity of presentation, only selected data are shown in Figures 3 to 6.

The velocity vector magnitude response relations of Equation 2 were established by calibrating the sum of the sensor mean Joulean energies (E_S^*) as a function of jet velocity, Figure 3, and yaw angle, Figure 4. Calibration results indicate that E_S^* is essentially a function of the magnitude of the cooling velocity, q. It can be concluded from Figure 4 that E_S^* is statistically independent of the yaw angle. This substantiates the King's law type of relation as advanced by Olin and Kiland and suggests that Equation 2 can be approximated without appreciable loss of accuracy by

$$E_S^* = A_S + B_S q^n \tag{6}$$

The yaw response relation (Equation 4) was determined by plotting the ratio of the sensor mean Joulean energies, E_R^*, as a function of yaw angle and jet velocity as shown in Figures 5 and 6, respectively. Calibration results indicate that E_R^* is linearly related to yaw angle, θ, and essentially independent of the magnitude of the cooling velocity, q. Since E_R^* is shown to be a function of θ alone, Equation 3 reduced to

$$E_R^* = A_R + B_R \tag{7}$$

In contrast, Olin and Kiland (9) found $E_R^* = A_R + B_R \theta^2$ gave the best agreement, whereas Spencer and Jones (11) used $E_R^* = A_R + B_R \sin \theta$. From Figure 5 it appears that if the calibration curve were broken into two curves in regions $\theta > 0$ and $\theta < 0$, the calibration statistics could be improved. The form

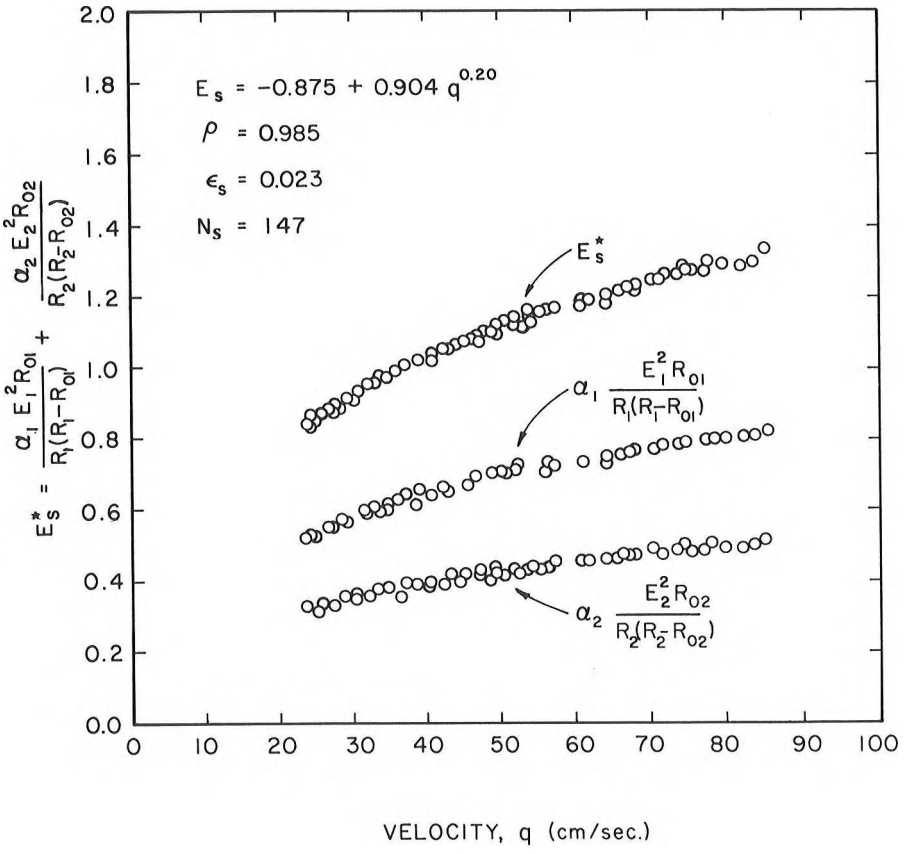

Figure 3. Variation of Joulean Energies sum with velocity, q, for $\theta = 0$.

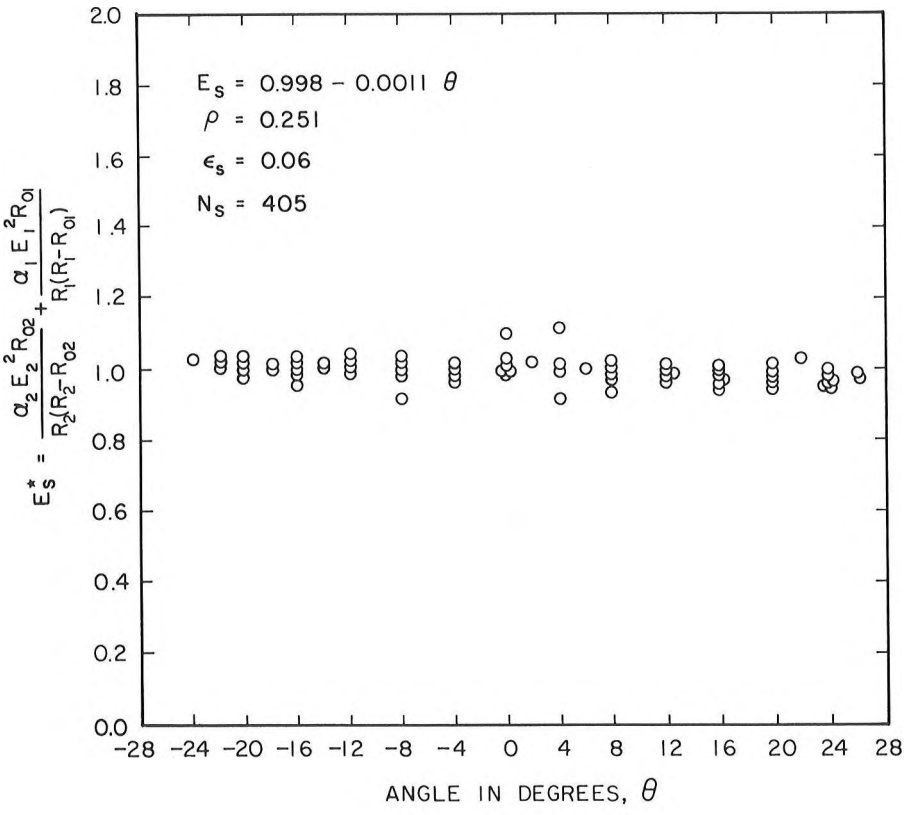

Figure 4. Variation of Joulean Energies sum with yaw angle, θ, for 25 cm/sec < q < 80 cm/sec.

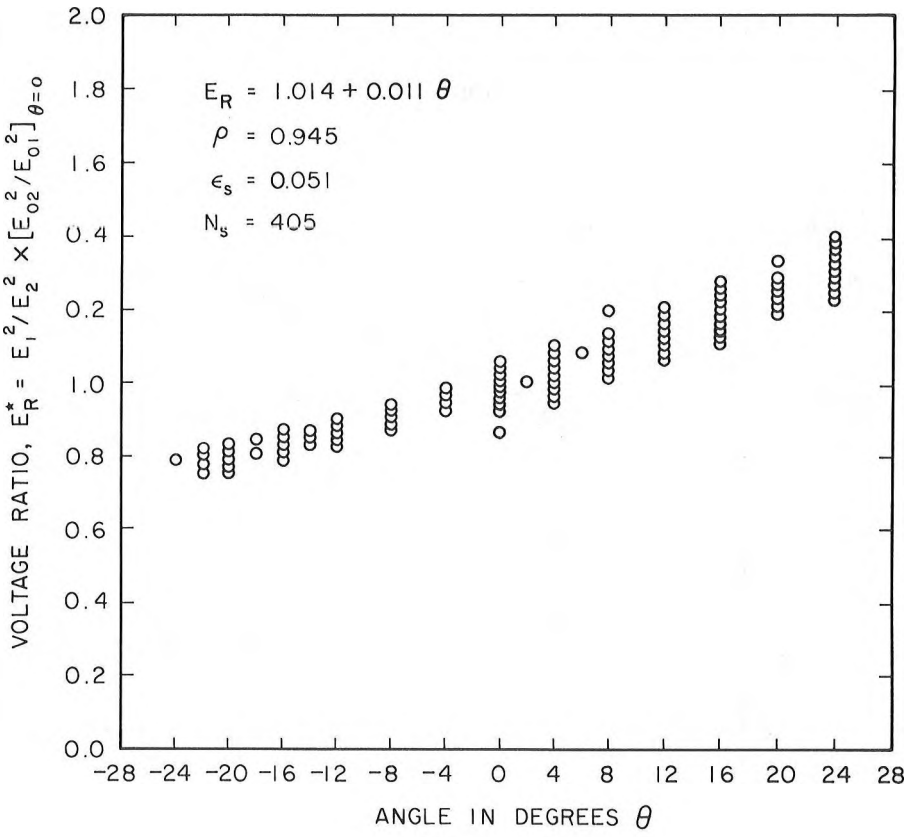

Figure 5. Variation of Joulean Energies ratio with yaw angle, θ, for 25 cm/sec < q < 80 cm/sec.

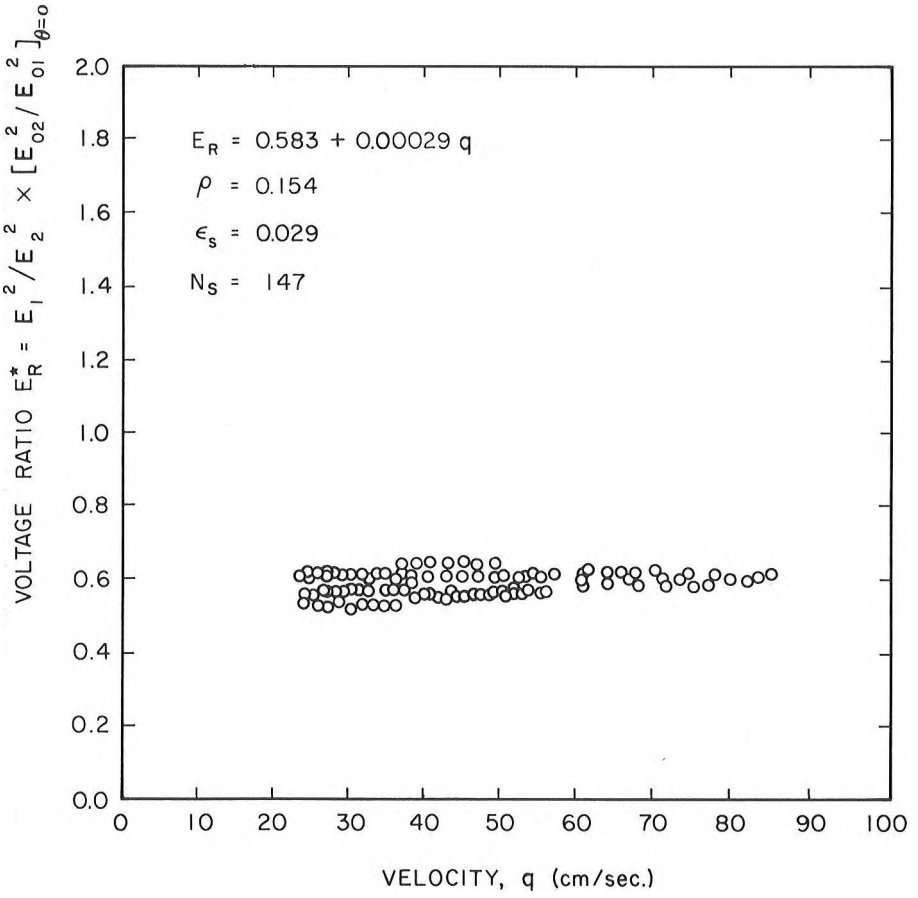

Figure 6. Variation of Joulean Energies ration with velocity, q.

suggested by Spencer and Jones gives approximately the same agreement as the linear expression, whereas the Olin and Kiland form did not agree with the two other forms. Figure 6 indicates that E_R^* is weakly dependent on the jet velocity; thus, using the maximum jet velocity U = 100 cm/sec. gives a maximum change of 4.5% in E_R^*. The scatter of the six independent calibrations appears greater for $E_R^* = f\{q, \theta\}$ than for $E_S^* = f\{q, \theta\}$. However, it should be noted that the standard error, ε, for $E_R^* = f\{\theta\}$ is less than the error of $E_S^* = \{q\}$.

DATA REDUCTION

The discrete time series of the longitudinal and vertical velocity fluctuations were constructed by digitizing the continuous recorded outputs of the SFHF sensor anemometer signals on an FM magnetic tape recorder and then playing the signals through an analog-to-digital (A/D) converter. The output from the A/D converter was transformed into the discrete velocity vector time series by using Equations 2 and 4 in a high-speed digital computer. The instantaneous longitudinal and vertical velocity components were determined by taking the sine and cosine of the instantaneous velocity vector, respectively. To resolve the instantaneous longitudinal velocity fluctuations, the mean value, $\overline{U}$, was subtracted from each of the instantaneous longitudinal values. The instantaneous Reynolds stress was computed from the product of the instantaneous velocities, u and v. The statistical moments, and covariance analysis were obtained using a high-speed computer (2).

EXPERIMENTAL RESULTS

Turbulent measurements were made in a smooth, 10 meter long, recirculating open channel flume. The flume was 20.4 cm wide by 20.4 cm deep and was carefully constructed of Plexiglas to insure hydraulically smooth flow conditions. All measurements were made on the flume center line, 6.9 meters downstream from the flume entrance section. For each selected flow discharge and flow depth, Y_o, the flume slope was adjusted by trial-and-error until uniform flow existed over the mid two-thirds of the flume. The flow Reynolds number, R_e, was based on the hydraulic radius and the bulk mean velocity, U_o. The gross hydraulic conditions for the results reported here are summarized in Table I. The wall shear stress, τ_o, or the corresponding shear velocity, U_*, was computed from the velocity gradient and cross checked with the Darcy-Weisbach friction coefficient.

Table I. Hydraulic Flow Conditions

Y_o cm	U_o cm/sec	R_e 10^4	U_* cm/sec	T °C
3.87	31.9	3.64	1.71	21.3
3.09	29.2	2.82	1.60	21.4
3.63	42.3	4.55	2.19	20.9

The mean velocity profiles obtained with the SFHF sensor were in good agreement with the Prandtl von Karman velocity distribution for dimensionless distances $y^+ > 10$ (not shown). However, as the wall was approached, the mean velocity profiles obtained from the SFHF sensor were considerably higher than the predicted values. The longitudinal and vertical turbulent intensities were in agreement with each other and with intensities determined in previous air and water studies (3, 5, 7, 8) for distances $y^+ > 10$, Figure 7. In the region $y^+ < 10$, the longitudinal, u'/U_*, SFHF sensor data are somewhat scattered and higher than those obtained in previous water studies (3, 4). The longitudinal velocity fluctuations peaked at 2.7 at $y^+ \approx 13$; these figures agree with those of both the air and water studies. The vertical turbulence intensities were in excellent agreement with Laufer's (7) results over the range $y^+ > 10$. SFHF sensor data for near the wall remained constant, $v'/U_* = 0.6$.

The discrepancy between the water data, and particularly between our data and those of Laufer for the region near the wall ($y^+ < 5$) stems from probe interference. It's a matter of conjecture as to whether the interference is due to direct thermal heat transfer from the adjacent split film sensor or the effects of local convective acceleration of the fluid probe and the wall. Other possible sources of error may be slight probe and split plane misalignment with the wall or the velocity gradient heat transfer on the split-film sensors. Another possible explanation for the high results in the intensities was the required extrapolation of the calibration curves necessitated by the low mean velocities near the wall. In comparing the mean velocity profiles and longitudinal turbulent intensities, it appears that probe interference becomes significant at $y^+ \approx 10$ or approximately 5 probe diameters from the wall.

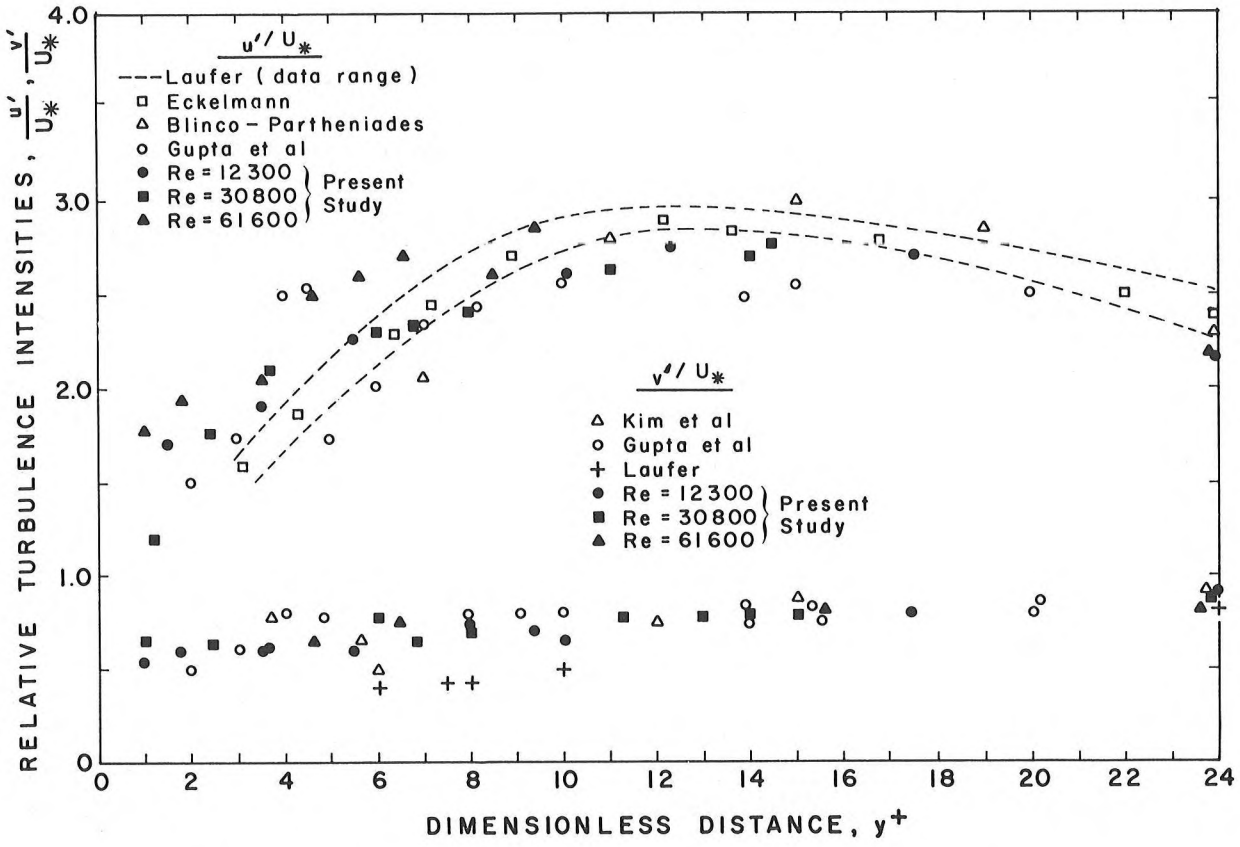

Figure 7. Comparison of Turbulence Data using SFHF sensor to previous air and water studies.

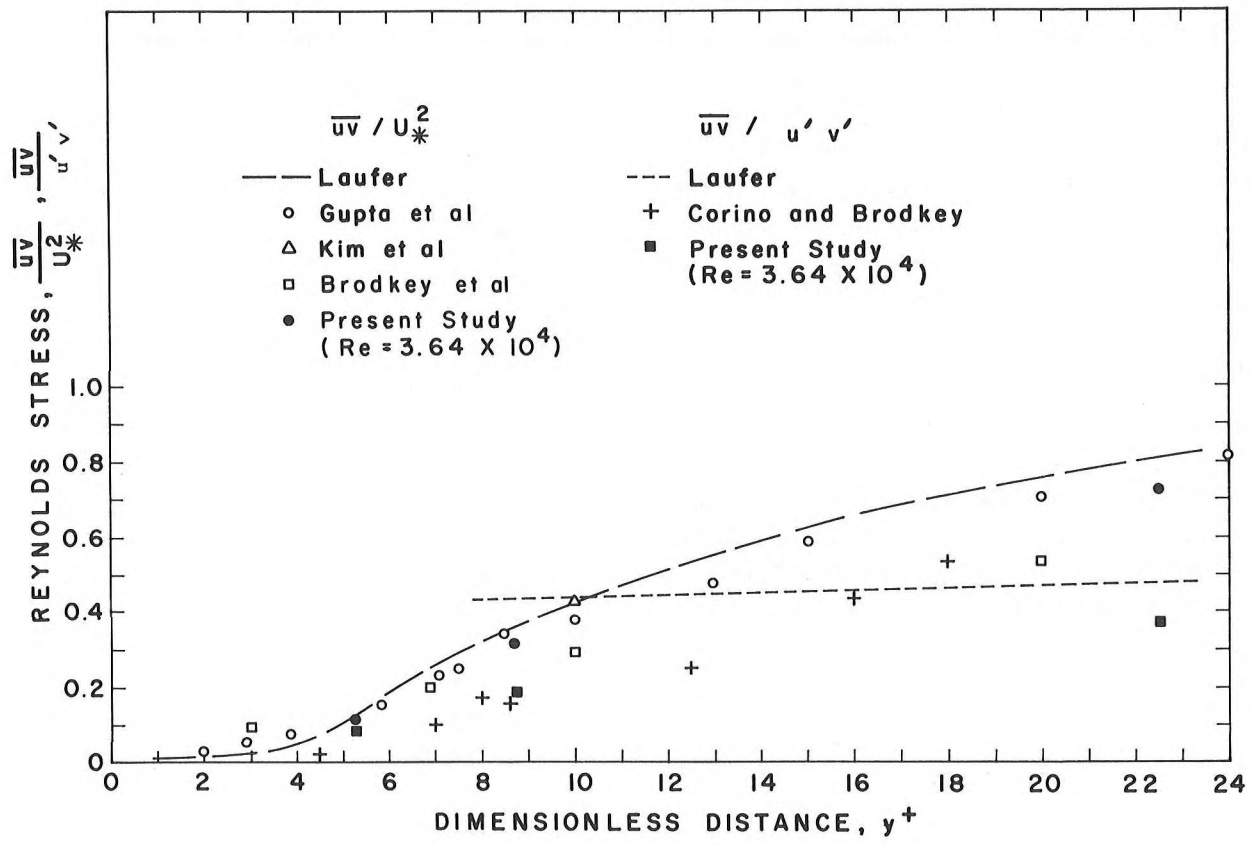

Figure 8. Variation of Reynolds stress with relative distance from the wall.

The mean Reynolds stress, $\overline{uv}$, obtained from the mean of the product of the velocity fluctuations u and v are presented in Figure 8. Here the Reynolds stress, $\overline{uv}$, has been normalized with respect to U_*^2 and the product of u' and v'. Both normalized Reynolds stress values are in excellent agreement with previous results (4, 7, 8). The distribution of $\overline{uv}/U_*^2$ from the edge of the viscous sublayer ($y^+ = 5$) through the buffer region is nearly linear. The Reynolds stress reaches a maximum value of 0.9 at approximately $y^+ = 30$ and remains essentially constant in the region $30 < y^+ < 100$ before decreasing (not shown). Thus, the location of maximum $\overline{uv}$ does not coincide with location of maximum turbulence intensity, u', or turbulence production $\overline{uv}\ \partial\overline{U}/\partial y$ (8). When the distribution of vertical turbulence intensity, v', is compared with the distribution of $\overline{uv}$, the latter seems similar in that both are increasing linearly in region $5 < y^+ < 30$. This would suggest the anti-correlation between u and v is more dependent on v than u.

An estimate of the frequency responses of the SFHF sensor was obtained by comparing signals from the SFHF sensor and a miniature boundary layer hot-film sensor. The miniature boundary layer sensor was of a cylindrical type (TSI Model 1270-10aW) which has a 0.026 mm sensor diameter and a 0.5 mm sensing length. The frequency responses of this type sensor have been shown to be greater than 1000 Hz which is at least six times greater than the highest expected frequency in this study (2). The two hot-film signals were compared both by digital and analog techniques. For small probe separations, the SFHF sensor output was indistinguishable from the miniature sensor when displayed on a dual beam oscilloscope. Both signals were found to be similar in wave form and spectral content.

Our intent in comparing the SFHF sensor data to those of previous air and water studies has been to show similarity in trends rather than absolute agreement. The apparent agreement with previous studies as to the two-dimensional statistical moments, covariance, other high correlations, and power spectra was used as the basis to judge use of the SFHF sensor as an instantaneous velocity vector transducer in shear flows.

SUMMARY AND CONCLUSIONS

Because of its small size and unique design the SFHF sensor has many distinct advantages over the conventional X-array hot-film sensor. The SFHF sensor's unique design, strength, and probe configuration allows for improved spatial definition of the two-dimensional velocity fields in liquid flows. The calibration response equations show that the magnitude of the velocity vector is a function of the sum of the sensor Joulean energies. Similarly, it was shown that SFHF sensor directional sensitivity is dependent on the ratio of the sensor and Joulean energies and independent of the local mean velocity. By using the developed response equations in a high-speed digital computer, we found the longitudinal and vertical turbulence intensities and Reynold stress to be in excellent agreement with those of previous studies for $y^+ > 10$. It was concluded that the SFHF sensor could measure the two-dimensional turbulent structure to within five probe diameters from the wall. The agreement between the data obtained in this study and those from previous studies shows that the stochastic structure of the two-dimensional velocity field can be accurately measured by the SFHF probe used as an instantaneous velocity vector transducer.

ACKNOWLEDGMENTS

The present research was made possible through a cooperative effort between the Department of Civil Engineering, Colorado State University, Agricultural Research Service, USDA, and the USDA Sedimentation Laboratory, Oxford, Mississippi.

Experimental assistance and suggestions from Dr. Didi Duma, Institute of Land Reclamation Research and Studies, Bucharest, Romania, and Dr. Chin-nan Shieh, graduate research assistant, Colorado State University, are gratefully acknowledged.

SYMBOLS

A_R, A_S	calibration constants
B_R, B_S	calibration constants
E_i	instantaneous anemometer voltage
E_R^*	ratio of instantaneous Joulean heating of split sensors
E_S^*	sum of instantaneous Joulean heating of split sensors

SYMBOLS(cont.)

N_s	data sample size
n	calibration exponent
q	instantaneous velocity vector
R_e	flow Reynolds number, $R_e = 4R_hU_o/\nu$
R_h	hydraulic radius
R_1, R_2	sensor resistance at operating temperature
R_{01}, R_{02}	sensor resistance at fluid temperature
T	temperature
U	local mean velocity and jet velocity
U_o	mean flow velocity over channel cross section
U_*	shear velocity
u	longitudinal instantaneous velocity about U
u'	root-mean-square of u
v	vertical instantaneous velocity
v'	root-mean-square of v
w	transverse instantaneous velocity
Y_o	depth of flow
y	distance up from the wall
y^+	dimensionless distance from the wall
α_1, α_2	coefficients of thermal resistance
γ	unit weight of fluid
ε	standard error
θ	yaw angle measured from the split plane
ν	kinematic viscosity of the fluid
ρ	regression correlation coefficient
ϕ	rotation angle

REFERENCES

1. Bakewell, H. P., and Lumley, J. L., "Viscous Sublayer and Adjacent Wall Region in Turbulent Pipe Flow", Phys. Fluids, 10, (1967).

2. Blinco, P. H., "Spatial Structure of the Viscous Sublayer", Ph.D. Thesis, Colorado State University, 1974

3. Blinco, P. H., and Partheniades, E., "Turbulence Characteristics in Free Surface Flows over Smooth and Rough Boundaries", Journal of Hydraulic Research, IAHR, 9, (1971).

4. Eckelmann, H., and Reichardt, H., "An Experimental Investigation in a Turbulent Channel Flow with a Thick Viscous Sublayer", Proc. of Symposium on Turbulence in Liquids, Cont. Educ. Series, University of Missouri-Rolla, 1971.

5. Gupta, A. K., and Kaplan, R. E., "Statistical Characteristics of Reynolds Stress in a Turbulent Boundary", Phys. Fluids, 15, (1972).

6. Klebanoff, P. S., "Characteristics of Turbulence in a Boundary Layer with Zero Pressure Gradient", NACA Report 1247, 1955.

7. Laufer, J., "The Structure of Turbulence in Fully Developed Pipe Flows", NACA Tech. Rep. 1175, 1954.

8. Laufer, J., "Investigation of Turbulent Flow in a Two-Dimensional Channel", NACA Tech. Rep. 1053 1953.

9. Olin, J. G., and Kiland, R. B., "Split-Film Anemometer Sensors for Three-Dimensional Velocity-Vector Measurement", Symposium on Aircraft Wake Turbulence, Seattle, Washington, 1970.

10. Sandborn, V. A., Resistance Temperature Transducers, Metrology Press, Fort Collins, pp. 235-236, 1972.

11. Spencer, B. W., and Jones, B. G., "Turbulence Measurements with the Split-Film Anemometer Probe", Proc. of Symposium on Turbulence in Liquids, Cont. Educ. Series, University of Missouri-Rolla, 1971.

DISCUSSION

T. J. Hanratty, University of Illinois: I was wondering if the large values of normal velocity close to the wall at small values of Y^+ could be ascribed to this heat loss or do you think they are real?

Sandborn: I imagine they are very much ascribed to the heat loss. It's the wall heat transfer effect coming in that we have not evaluated at this time.

Hanratty: That may indicate that the loss is affecting the data to about $Y^+ = 8$ or 10. I am very interested in the turbulent velocity normal to the wall and if these data are accurate, I'm pleased to have them. If they're inaccurate then please give an indication how close you can get to the wall before you are confronted with these thermal effects.

Sandborn: I think my comment is that the wall measurements are indefensible at this point. They are what came out without corrections for the wall involved.

Blinco: The approximate thickness of the viscous sublayer was 0.30 mm and the sensor diameter was 0.153 mm. As mentioned the mean velocity profile obtained was in general agreement over the range $Y^+ \geq 10$. In the region $Y^+ < 10$, the mean velocity estimates were found to increase progressively relative to the predicted values as the wall is approached. No attempt was made to determine the relative influence of free convective heat transfer or to correct for heat loss to the wall. Any corrective procedure in the region $Y^+ < 10$ would be dubious in view of the relative size of the sensor to the sublayer thickness. Also, Spencer and Jones of the University of Illinois have shown in air that this type of sensor is capable of turbulence measurement close to a wall. Their results showed that probe-wall interference started approximately 10 sensor diameters from the wall.

R. N. Houze, Purdue University: I was wondering if you had investigated the effect of the probe in a shear field where you have a velocity gradient. The top of the probe is going to see a different mean velocity than the bottom. Is this going to have any significant effect on your data?

Sandborn: In regard to the shear stress over the probe, you probably do have an effect, and I think we have shown it with hot wires, but I think the answer here would be no. Hopefully by having a very small diameter, 0.153 mm you don't have as big a problem as you would have with the yawed wire.

Blinco: The closest measurement to the wall was really 3 sensor diameters, which would be about 0.018 inch on the center line of the sensor.

G. K. Patterson, University of Missouri-Rolla: Was that about $Y^+ = 5$?

Blinco: Yes, I think that Y^+ value was about 6. In view of the previous remarks I'm not suggesting by its inclusion in the presented material that measurements this close are correct. The value was obtained because we attempted to obtain the time-space correlation structure with a flush-mounted sensor located downstream from the split-film sensor.

Patterson: My other question has to do with this - you seem to have gotten pretty fair checks between the data you obtained at least for the U'-data, the fluctuating velocity in the longitudinal direction, with data that other people have gotten with other kinds of sensors. I have done some experiments with the same sensor that you have, same size and everything, and in a pipe where I can very well characterize what the shear stress at the wall is by simply measuring the pressure drop. Now when I compared my data with other data in the same way you did, my U'-data always came out to be about 20% low. I have been trying to resolve this but I haven't succeeded. I wonder if there is anything in your data and the treatment that might give a clue to how this could happen or what would make this data consistent. For instance, how did you get your U*?

Blinco: This is a difficult question. I don't know how you analyzed your data. I'm suggesting that if you use our approach - if you digitized point by point using the heat transfer relations as presented and simultaneously analyzed the data using it as X-wire sensor - one might be able to determine the difficulties you encountered. Unfortunately, we did not attempt to obtain results using the analog method. As for your second question the boundary shear stress was obtained by measuring the energy gradient of the flow.

Patterson: I analyzed the data more from the X-wire standpoint using strictly analog equipment and there is a possibility that this could be called a calibration type problem.

Blinco: I would like to mention one thing else. The calibrations that you saw were ensemble averages of six calibrations over 16 days. The individual calibrations are significantly superior to the six ensemble average calibration presented here. Here, we wanted to demonstrate how effectively this sensor could hold its calibration over a short time period provided that water conditions remain constant.